Optical Materials 75 (2018) 662–665

Contents lists available at ScienceDirect

Optical Materials

journal homepage: www.elsevier.com/locate/optmat

# Structural properties of $Eu^{3+}$ doped $Gd_2Zr_2O_7$ nanopowders: Far-infrared spectroscopy

J. Mitrić [a, *], J. Križan [b], J. Trajić [c], G. Križan [b], M. Romčević [c], N. Paunović [c], B. Vasić [c], N. Romčević [c]

[a] School of Computing, University Union, Knez Mihailova 6, Belgrade 11 000, Serbia
[b] AMI, d. o. o., Ptuj, Slovenia
[c] Institute of Physics, University of Belgrade, Pregrevica 118, 11080 Belgrade, Serbia

ARTICLE INFO

*Article history:*
Received 2 October 2017
Accepted 15 November 2017
Available online 23 November 2017

*Keywords:*
$Gd_2Zr_2O_7$
$Eu^{3+}$
Nanopowders
Phonons
Light absorption and reflection

ABSTRACT

The Solution Combustion Synthesis (SCS) method was used to prepare nanopowders of europium doped cubic $Gd_2Zr_2O_7$ nanopowders. The surface of the samples have been investigated using atomic force spectroscopy (AFM) and far-infrared spectroscopy (FIR). Far-infrared reflectivity spectra of $Eu^{3+}$ doped $Gd_2Zr_2O_7$ nanopowders were measured at room temperature in spectral region between 80 and 650 $cm^{-1}$. The Maxwell–Garnet formula was used to model dielectric function of $Eu^{3+}$ doped $Gd_2Zr_2O_7$ nanopowders as mixtures of homogenous spherical inclusions in air.



## 1. Introduction

$A_2B_2O_7$ type of pyrochlores are important class of materials because of their diverse scientific and technological applications like in nuclear waste storage [1], electro/photo catalysis [2,3], luminescence [3], $CO_2$ hemisorption [4], photoluminescence hosts [5], topological Mott insulator [6] etc.

Pyrochlore oxides which occur in various crystalline phases, manifest numerous interesting and important physicochemical properties which make them eligible for potential hosts for the chemical substitution [7].

Rare earth based zirconates ($Re_2Zr_2O_7$) pyrochlores have wide scientific and technological applications as: potential thermal barrier coatings (TBC), high temperature heating devices or luminescence hosts [8].

Among all rare earth based pyrochlores, $Gd_2Zr_2O_7$ stands out as a material with a distinctively low thermal conductivity and high phase stability [9]. Besides that, $Gd_2Zr_2O_7$ could be an excellent candidate for potential photoactive materials [10].

As shown through our previous work [4,11], there are two different crystal structures for $Gd_2Zr_2O_7$, pyrochlore and the fluorite type.

Rare earth ions are widely used as activators for various phosphors and other organic and inorganic luminescent materials, because they offer high color purity, high luminescence lifetime and also a narrow emission profile, thanks to its optically active 4f electrons which are strongly shielded from the rest of ions by the other 5s and 5p shells [12].

Among all lanthanides, $Eu^{3+}$ ion is in advantage as a dopant ion for structural probing, as well as for synthesis of red light emitting phosphor [8]. The reason this ion is a useful spectroscopic probe is because of its main source of luminescence - single level, $^5D_0$ state, which prevents the convolution of overlapping emission peaks from different levels [13]. Also, doping any aliovalent ion in these oxides is not only used for structural probing, but it could also generate significant changes in photophysical behavior of those materials in such way that doping creates various kinds of defects like ion/oxygen vacancies, which can alter the band gap of materials, i.e. photophysical characteristics of one material. Particularly for $Gd_2Zr_2O_7$, it is proven that efficient doping results in tuning of thermal [14], electrical [15], optical [4] and other properties.

In this paper, we present the results obtained by using far – infrared spectroscopy (FIR) to study optical properties of the $Eu^{3+}$ doped $Gd_2Zr_2O_7$ nanopowders which were prepared by the Solution Combustion Synthesis (SCS) method. The dielectric function of $Eu^{3+}$ doped $Gd_2Zr_2O_7$ nanopowder is modeled as a mixture of

* Corresponding author.
*E-mail address:* jmitric@ipb.ac.rs (J. Mitrić).

https://doi.org/10.1016/j.optmat.2017.11.026
0925-3467/

homogenous spherical inclusions in air, by the Maxwell-Garnet formula.

## 2. Sample and characterization

Europium doped cubic $Gd_2Zr_2O_7$ nanopowders were prepared by Solution Combustion Synthesis (SCS) method. Starting chemicals $Gd(NO_3)\cdot 6H_2O$, $Zr(NO_3)_2\cdot H_2O$, $Eu(NO_3)\cdot 6H_2O$ with the purity of 99,99% were purchased from ABCR, $Gd_2O_2$ (99,9%) from the NOAH Technologies and urea $(NH_2)_2CO$ from Sigma-Aldrich.

Due to its simplicity and low cost of the synthesis procedures and possibility of tailoring the size and morphology of particles, the flame combustion process is the most frequently used. After the synthesis, the nanopowder was annealed, in order to achieve the full crystallinity, in air atmosphere at 1200 °C for 2 h. The $Eu^{3+}$ concentration in $Gd_2Zr_2O_7$ was 2 mol%. The morphology analysis of the synthesized materials indicates the irregular crystallite size distribution and existence of agglomerated grains which are in the submicron size.

In our previous work [4,11] we performed X – ray powder diffraction (XRD) and photoluminescence measurements of the same material. XRD analysis confirmed that sample was crystallized in fluorite (F) type structure (space group Fm3m). The photoluminescence spectra showed a number of electronic transitions, among them were those at 705 nm and 713 nm ($^5D_0 - {}^7F_4$), 654 nm ($^5D_0 - {}^7F_3$), 630 and 611 nm ($^5D_0 - {}^7F_2$), 593 nm ($^5D_0 - {}^7F_1$), 584 nm ($^5D_0/{}^5D_1 - {}^7F_1$) and 578 nm ($^5D_0/{}^5D_1 - {}^7F_0$).

The Raman spectra of $Eu^{3+}$ doped $Gd_2Zr_2O_7$ nanopowders were measured. We registered three phonons at 177 $cm^{-1}$, 268 $cm^{-1}$ and 592 $cm^{-1}$, as well as their overtones at 354 $cm^{-1}$, 445 $cm^{-1}$, 708 $cm^{-1}$, 1062 $cm^{-1}$, 1184 $cm^{-1}$, ~1530 $cm^{-1}$ and ~1720 $cm^{-1}$. The phonon at 592 $cm^{-1}$ was already known to be characteristic for $Gd_2Zr_2O_7$ fluorite – type structure, and we found that other two phonon positions to be characteristic with the observed electron – phonon observed interaction and that the registered multiphonon processes were a consequence of miniaturization that further induces changes in electronic structure of $Eu^{3+}$ doped $Gd_2Zr_2O_7$ nanopowders. All the above mentioned results will be useful in the far – infrared spectroscopy analysis of $Eu^{3+}$ doped $Gd_2Zr_2O_7$ nanopowders.

## 3. Results and analysis

### 3.1. AFM

Atomic force microscopy (AFM) measurements were done using NTEGRA Prima system from NT-MDT at room temperature and ambient conditions. Imaging was done in tapping mode using NSG01 probes. Phase lag of AFM cantilever was recorded simultaneously during tapping mode imaging.

Two dimensional and three dimensional topography of the sample surface are shown in Fig. 1(a) and (b), respectively (scan size is 5 × 5 $\mu m^2$). As can be seen, the surface is rather flat with characteristic holes represented with dark color. Cross section of one characteristic hole (along dashed line in Fig. 1(a)) is given in the inset of Fig. 1(a). Hole width and depth are around 1 μm and 200 nm, respectively. Apart from this holes, the sample surface consists of small grains. They are better visualized in Fig. 1(c) and (d) showing the topography and phase contrast image of a zoomed part (scan size is 1 × 1 $\mu m^2$). Grains are clearly visible, especially

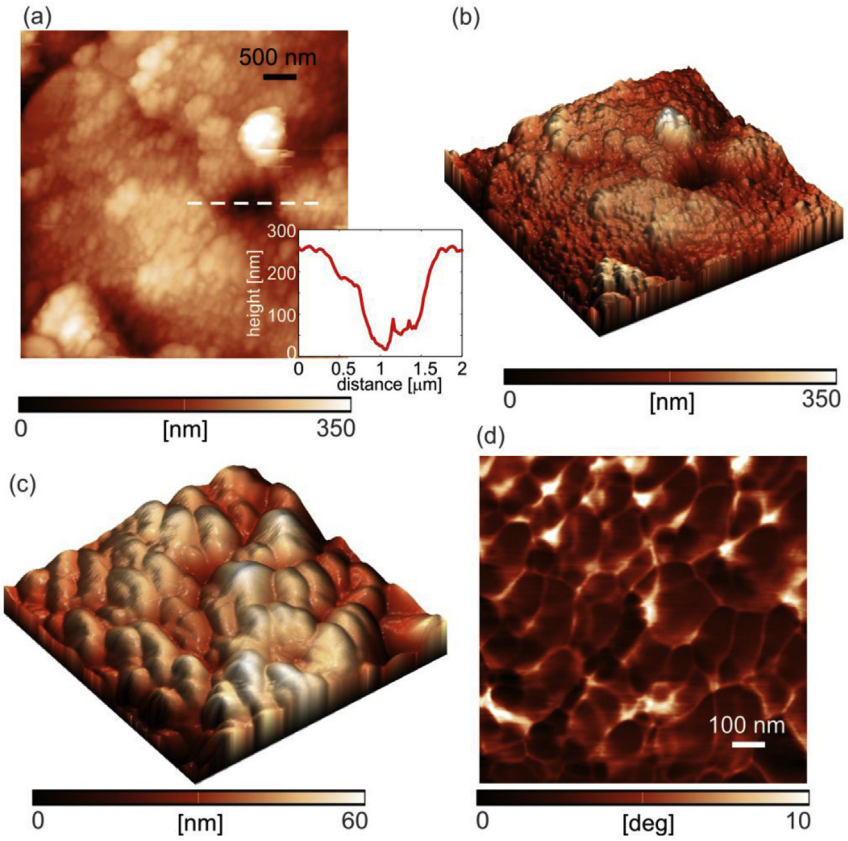


**Fig. 1.** (a) Two-dimensional and (b) three-dimensional topography of the sample surface. The inset in part (a) shows the cross-section along the corresponding dashed line. (c) Three-dimensional topography and (b) corresponding phase contrast image of a zoomed region from part (a).

grain boundaries in the phase contrast image since the phase is very sensitive to abrupt changes in the topography. Dispersion of grain size is rather wide, but still we can conclude that the characteristic grain size is in the order of 100 nm.

### 3.2. Far-infrared spectroscopy

The infrared reflectivity measurements were performed at room temperature with a BOMEM DA-8 Fourier-transform infrared spectrometer. A Hyper beamsplitter and deuterated triglycine sulfate (DTGS) pyroelectric detector were used to cover the wave number region from 80 to 650 $cm^{-1}$. Spectra were collected with 2 $cm^{-1}$ resolution and with 500 interferometer scans added for each spectrum.

When visible light, λ, interacts with semiconducting nanoparticles (characteristic size d, dielectric function $\varepsilon_2$) which are distributed in a medium with the dielectric constant $\varepsilon_1$ in the limit $\lambda \gg d$, the heterogeneous composite can be treated as a homogeneous medium and effective medium theory is applied. There are many mixing models for the effective dielectric permittivity of such mixture [16]. Since our samples are well defined and separated nanosized grains, we used Maxwell-Garnet model for present case. For the spherical inclusions case, the prediction of the effective permittivity of mixture, $\varepsilon_{eff}$, according to the Maxwell-Garnet mixing rule is [17]:

$$\varepsilon_{eff} = \varepsilon_1 + 3f\varepsilon_1 \frac{\varepsilon_2 - \varepsilon_1}{\varepsilon_2 + 2\varepsilon_1 - f(\varepsilon_1 - \varepsilon_2)} \quad (1)$$

Here, spheres of permittivity $\varepsilon_2$ are located randomly in homogeneous environment $\varepsilon_1$ and occupy a volume fraction f. The observed nanoparticles are situated in air, therefore the $\varepsilon_1$ is 1. For dielectrical function of observing nanoparticles ($\varepsilon_2$) we used the standard model [18]:

$$\varepsilon_2(\omega) = \varepsilon_\infty \left( \prod_{k=1}^{n} \frac{\omega_{LOk}^2 - \omega^2 + i\gamma_{LOk}\omega}{\omega_{TOk}^2 - \omega^2 + i\gamma_{TOk}\omega} - \frac{\omega_P^2}{\omega(\omega - i\tau^{-1})} \right) \quad (2)$$

where $\varepsilon_\infty$ is the bound charge contribution and it is assumed to be a constant, $\omega_{TOk}$ and $\omega_{LOk}$ are transverse and longitudinal frequencies, $\gamma_{TOk}$, and $\gamma_{LOk}$ are their dampings, $\omega_P$ is the plasma frequency and $\tau$ is the free carrier relaxation time. The first term in (2) is the lattice contribution, whereas the second term is the Drude expression for the free carrier contribution to the dielectric constant. In this case, we will consider $\omega_{TOk}$ as a characteristic frequency of material ($\nu_k$), and we will link $\omega_{LOk}$ with oscillator strength ($S_k \sim \omega_{LOk}^2 - \omega_{TOk}^2$) which does not have big influence on discussion.

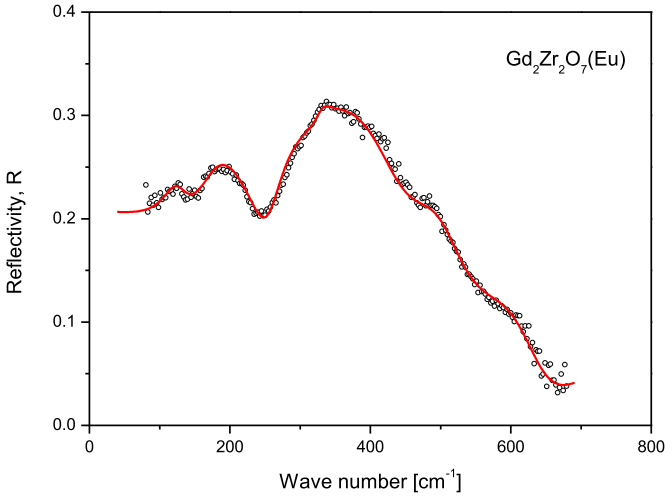


**Fig. 2.** Far – infrared reflection spectra of $Eu^{3+}$ doped $Gd_2Zr_2O_7$ nanopowder. The experimental data are represented by circles. The solid lines are the calculated spectra obtained with the parameter values given in Table 1 and the fitting procedure based on the model given by Eqs. (1) and (2).

The far-infrared spectra of $Eu^{3+}$ doped $Gd_2Zr_2O_7$ nanopowders, in the spectral range of 80–650 $cm^{-1}$, at room temperature, are presented in Fig. 2. The experimental data are presented by circles, while the solid lines are calculated spectra obtained by a fitting procedure based on the previously presented model. In Table 1 the best fit parameters are presented. Values for $Eu^{3+}$ doped $Gd_2Zr_2O_7$ single crystal are taken from literature [11,19–22].

McCauley [23], and Vandenborre [24] came to the result that of the total number of 26 normal modes ($\Gamma = A_{1g} + E_g + 2F_{1g} + 4F_{2g} + 3A_{2u} + 3E_u + \mathbf{8F_{1u}} + 4F_{2u}$) only those of $F_{1u}$ vibrations are active in the IR absorption. One of the eight $F_{1u}$ modes is associated with three degrees of translation of the unit cell and refers to the acoustic branch of the crystal vibrations and thus analysis predict 7 IR – active optic modes [22]. Our results confirm all of the seven active vibrations and their assignations are shown in Table 1 and also indicate that anharmonicity factors are not significant. The analysis [23,24] also predicts that six vibrations of the types $A_{1g}$, $E_g$ and $4F_{2g}$ are Raman – active modes. As per the selection rules, the remaining modes ($F_{1g}$, $A_{2u}$, $E_u$ and $F_{2u}$) are inactive both in the IR and Raman spectra. According to the group-theoretical analysis, all the atoms of the crystal lattice are involved in the seven IR active $F_{1u}$ vibrations (and six Raman – active modes) of the pyrochlore [22–24].

Following other authors' and our previous work [11,25] we started our analysis from the bulk material, considering that understanding bulk properties will lead to better understanding of properties of small particles, and therefore, as a result we expect the bulk modes to be shifted and broadened.

All modes are shifted compared to literature data. We believe that this is not because of the doping with $Eu^{3+}$ and that in relatively small concentrations/amounts, doping did not induce changes in phonon spectra of $Gd_2Zr_2O_7$ [26]. We confirm our previous work [11] where we used Raman spectroscopy to obtain modes at 177 $cm^{-1}$ and 268 $cm^{-1}$ which noticeably differed from results obtained by many other authors who claimed that these modes occur at ~140 $cm^{-1}$ (O-A-O vibrations) and ~220 $cm^{-1}$ (O-B-O vibrations), respectively. Using FIR spectroscopy we obtained significant modes at 175 $cm^{-1}$ and 255 $cm^{-1}$ which describe O-A-O and O-B-O vibrations, respectively. The reason for this shift, as we believe, is electron – phonon interaction which led to the breakdown of the selection rules and appearance of the new phonons in fluorite structure $Gd_2Zr_2O_7$:Eu spectrum [11].

Interesting thing is, FIR spectrum shows two modes characteristic for pyrochlore type of structure, at 365 $cm^{-1}$ and 490 $cm^{-1}$, although they are weak [19]. These two modes correspond to the vibrations of $GdO_8$ and $ZrO_6$ polyhedra, respectively. This confirm some earlier thoughts of P phase and F phase co-existing in the sample [19]. As it was said earlier [4,11], $Gd_2Zr_2O_7$ has two isometric structures, disordered fluorite (F) and ordered pyrochlore (P). In general, disordered fluorite structure type for this compound is confirmed [4]. But, it is also known that $Ln_2Zr_2O_7$ (Ln = elements of lanthanide series) have a pyrochlore-type structure stable at low temperature [19]. The Raman activity allowed for the pyrochlore structure results from oxygen vibrations, and only four bands are observed in the Raman spectra of $Ln_2Zr_2O_7$ pyrochlore-type compounds (Table 1 [21]). In the ordered structure there is no evidence of the significant band at 125 $cm^{-1}$, like our FIR spectrum shows.

**Table 1**
Best fit parameters of far – infrared spectra of $Eu^{3+}$ doped $Gd_2Zr_2O_7$.

| Exp. results: $Gd_2Zr_2O_7$: $Eu^{3+}$ nanopowder | Literature: $Gd_2Zr_2O_7$: $Eu^{3+}$ single crystal | Assignment |
|---|---|---|
| 50 | – | $\nu_7$: O′-Gd-O′ bending vibrations |
| 126 | – | $\nu_6$: Gd-$ZrO_6$ streching vibrations |
| 175 | 177 [11] | $\nu_5$: O-Gd-O bending vibrations |
| 255 | 268 [11] | $\nu_4$: O-Zr-O bending vibrations |
| 330 | 310 [20], 315 [21] | $\nu_3$: Zr-O + O-Zr-O vibrational mode (O-Zr-O bending) |
| 365 | 370 [19], 400 [21] | $\nu_2$: vibrations of $GdO_8$ polyhedra |
| 490 | 500 [19], 538 [21] | $\nu_1$: Zr-O stretching vibration, vibrations of $ZrO_6$ polyhedra |
| 610 | 599 [20], 592 [21] | $E_g$: Zr-O′ stretching vibration |

The thing is, for $Ln_2Zr_2O_7$ compounds, an order – disorder transition pyrochlore ↔ defective fluorite may occur when the temperature is raised [21]. This confirms that in $Gd_2Zr_2O_7$:Eu nanopowder P- and F- phase coexist. At first, this is not in agreement with XRD results for $Gd_2Zr_2O_7$:Eu nanopowder [4], but using FIR spectroscopy in reflectivity mode, we concern mainly the surface of material and coexistence of two phases is characteristic for the surface, but not for the general structure which is generally investigated using XRD.

Modes at 330 $cm^{-1}$ and 610 $cm^{-1}$ are clearly visible in both F phase and P phase spectra [20] and they correspond to Zr-O + O-Zr-O vibrational mode.

The rest of well known IR active vibrations, O-Gd-O and O′-Gd-O′ (O′ represents the 8(a) site oxide ion [27,28]) bending vibrations, are not yet assigned for Gd - zirconates. We assume that these vibrations correspond to 50 $cm^{-1}$, 126 $cm^{-1}$ modes, respectively. The mode at 50 $cm^{-1}$ clearly could not be obtained with our spectrometer which works in 80–650 $cm^{-1}$ region, but that mode is well-suited to the fitting procedure based on the model given by Eqs. (1) and (2). Value of 50 $cm^{-1}$ for Gd-zirconate is expected, regarding [[22], pg. 78, Table VII] which shows O′-Gd-O′ assignments for lanthanide series from La to Sm, but not for the Gd. We find answer in the isotope effect. The change in spectrum is conditioned with the mass of nuclei, and if the mass of some element is greater, spectral lines will move to lower values of wave number. Therefore, considering the increase in mass from La to Gd, we assume that previously unknown wave number value of O′-Gd-O′ vibration for Gd-zirconates corresponds to our result of 50 $cm^{-1}$ (value of wave numbers from La to Gd are decreasing). We also use isotopic shift to explain the 126 $cm^{-1}$ for which we assume corresponds to O-Gd-O vibration band and it also may suggest the possibility of a lowered local symmetry for some crystallographic sites [24] (that is in agreement with our assumptions with order ↔ disorder transition).

## 4. Conclusion

In this paper far-infrared reflectivity measurements were used to obtain phonon properties of $Eu^{3+}$ doped $Gd_2Zr_2O_7$ nanopowders. We registered phonons of both isomeric structures characteristic for $Gd_2Zr_2O_7$ nanopowder and concluded coexistence of these two phases on the surface of the material, whereas fluorite structure is typical for the general structure. Low frequency modes were registered and regarding isotope effect they have been assigned.

## Acknowledgments

This work was supported by Serbian Ministry of Education, Science and Technological Development under Project III45003.

## References

[1] C. Fischer, S. Finkeldei, F. Brandt, D. Bosbach, A. Luttge, Direct measurement of surface dissolution rates in potential nuclear waste forms: the example of pyrochlore, ACS Appl. Mater. Interfaces 7 (32) (2015) 17857–17865.
[2] M.C. Hsieh, G.C. Wu, W.G. Liu, W.A. Goddard, C.M. Yang, Nanocomposites of tantalum-based pyrochlore and indium hydroxide showing high and stable photocatalytic activities for overall water splitting and carbon dioxide reduction, Angew. Chem. Int. Ed. 53 (51) (2014) 14216–14220.
[3] J. Parrondo, M. George, C. Capuano, K.E. Ayers, V. Ramani, Pyrochlore electrocatalysts for efficient alkaline water electrolysis, J. Mater. Chem. A 3 (20) (2015) 10819–10828.
[4] M.S. Rabasovic, D. Sevic, J. Krizan, M. Terzic, J. Mozina, B. Marinkovic, N.R.M. Mitric, M.D. Rabasovic, Characterization and luminescent properties of $Eu^{3+}$ doped $Gd_2Zr_2O_7$ nanopowders, J. Alloys Compd. 622 (3) (2014) 292–295.
[5] R.J. Walker, et al., Surface termination and CO2 adsorption onto bismuth pyrochlore oxides, Chem. Mater. 28 (1) (2016) 90–96.
[6] T. Kondo, et al., Quadratic Fermi node in a 3D strongly correlated semimetal, Nat. Commun. 6 (2015) 10042.
[7] S.K. Gupta, P.S. Ghosh, C. Reghukumar, N. Pathak, R.M. Kadam, Experimental and theoretical approach to account for green luminescence from $Gd_2Zr_2O_7$ pyrochlore: exploring the site occupancy and origin of host-dopant energy transfer in $Gd_2Zr_2O_7$, RSC Adv. 6 (50) (2016) 44908–44920.
[8] J. Wu, et al., Thermal-barrier-coating applications, J. Am. Ceram. Soc. 35 (2002) 3031–3035.
[9] L. Wang, J.I. Eldridge, S.M. Guo, Thermal radiation properties of plasma-sprayed $Gd_2Zr_2O_7$ thermal barrier coatings, Scr. Mater. 69 (9) (2013) 674–677.
[10] K.-J. Hu, Z.-G. Liu, J.-Y. Wang, T. Wang, J.-H. Ouyang, Synthesis and photoluminescence properties of $Eu^{3+}$- doped $Gd_2Zr_2O_7$, Mater. Lett. 89 (2012) 276–278.
[11] G. Križan, M. Gilić, J.L. Ristić - Đurović, J. Trajić, M. Romčević, J. Križan, B. Hadžić, B. Vasić, N. Romčević, Raman Spectroscopy and electron - phonon coupling in $Eu^{3+}$ doped $Gd_2Zr_2O_7$ nanopowders, Opt. Mater. 73 (2017) 541–544.
[12] Y.S. Chang, H.J. Lin, Y.L. Chai, Y.C. Li, Preparation and luminescent properties of europium-activated $YInGe_2O_7$ phosphors, J. Alloys Compd. 460 (1–2) (2008) 421–425.
[13] W. Zheng, P. Huang, D. Tu, E. Ma, H. Zhu, X. Chen, Lanthanide-doped upconversion nano-bioprobes: electronic structures, optical properties, and biodetection, Chem. Soc. Rev. (6) (2015) 1379–1415.
[14] K.S. Lee, K.I. Jung, Y.S. Heo, T.W. Kim, Y.G. Jung, U. Paik, Thermal and mechanical properties of sintered bodies and EB-PVD layers of $Y_2O_3$ added $Gd_2Zr_2O_7$ ceramics for thermal barrier coatings, J. Alloys Compd. 507 (2) (2010) 448–455.
[15] X.L. Xia, Z.G. Liu, J.H. Ouyang, S. Gao, X.M. Liu, Effect of Ce substitution for Zr on electrical property of fluorite-type $Gd_2Zr_2O_7$, Solid State Sci. 13 (6) (2011) 1328–1333.
[16] J. Trajić, M.S. Rabasović, S. Savić-Šević, D. Šević, B. Babić, M. Romčević, J.L. Ristić-Djurović, N. Paunović, J. Križan, N. Romčević, Far-infrared spectra of dysprosium doped yttrium aluminium garnet nanopowder, Infrared Phys. Technol. 77 (2016) 226–229.
[17] J.C.M. Garnett, Colours in metal glasses and in metallic films i (1904).
[18] I.J. Uhanov, Opt. Svojstva Poluprovodnikov, Nauka, Moskva, 1977.
[19] L. Zhou, et al., Thermal-driven fluorite–pyrochlore–fluorite phase transitions of $Gd_2Zr_2O_7$ ceramics probed in large range of sintering temperature, Metall. Mater. Trans. A Phys. Metall. Mater. Sci. (2015) 1–8.
[20] T. Moriga, S. Emura, A. Yoshiasa, S. Kikkawa, F. Kanamaru, X-ray and Raman study on coordination states of fluorite- and pyrochlore- type compounds in the system $ZrO_2$-$Gd_2O_3$ 50 (1990) 357–361.
[21] D. Michel, M.P.Y. Jorba, R. Collongues, Study by Raman spectroscopy of order-disorder phenomena occurring in some binary oxides with fluorite-related structures, J. Raman Spectrosc. 5 (2) (1976) 163–180.
[22] M.A. Subramanian, G. Aravamudan, G.V. Subba Rao, Oxide pyrochlores - a review, Prog. Solid State Chem. 15 (2) (1983) 55–143.
[23] R.A. McCauley, Infrared-absorption characteristics of the pyrochlore structure, J. Opt. Soc. Am. 63 (6) (1973) 721.
[24] R.A. McCauley, Infrared-absorption characteristics of the pyrochlore structure, J. Opt. Soc. Am. 63 (6) (1973) 721.
[25] C.S.S.R. Kumar, Raman Spectroscopy for Nanomaterials Characterization, Springer-Verlag, Berlin Heidelberg, 2012.
[26] X.L. Xia, J.H. Ouyang, Z.G. Liu, Electrical properties of gadolinium-europium zirconate ceramics, J. Am. Ceram. Soc. 93 (4) (2010) 1074–1080.
[27] M.T. Vandenborre, E. Husson, J.P. Chatry, D. Michel, Rare-earth titanates and stannates of pyrochlore structure; vibrational spectra and force fields, J. Raman Spectrosc. 14 (2) (1983) 63–71.
[28] M.T. Vandenborre, E. Husson, Comparison of the force field in various pyrochlore families II. Phases presenting structural defects, J. Solid State Chem. 5359 (1984) 253–262.